

Traceable Nanoparticles with Dual Targeting and ROS Response for RNAi-Based Immunotherapy of Intracranial Glioblastoma Treatment

Chenmeng Qiao, Jun Yang, Qi Shen, Ruiyuan Liu, Yanhui Li, Yuanjie Shi, Jingli Chen, Yanqin Shen, Zuobing Xiao, Jie Weng,* and Xin Zhang*

The chemotherapy of glioblastoma is severely hindered by the immunosuppressive tumor microenvironment, especially the tumor growth factor β (TGF- β), an immunosuppressive cytokine. In this study, it is proposed to employ RNAi-based immunomodulation to modify the tumor immune microenvironment and improve the effect of chemotherapy. Herein, a nanotheranostic system (Angiopep LipoPCB(Temozolomide+BAP/siTGF- β), ALBTA) with dual targeting and ROS response is established for intracranial glioblastoma treatment. The traceable nanoparticles exhibit strong siRNA condensation, high drug loading efficiency, good serum stability, and magnetic property. They can efficiently cross the blood–brain barrier and target to glioblastoma cells via receptor-mediated transcytosis. The zwitterionic lipid (distearoyl phosphoethanol-amine-polycarboxybetaine lipid) in ALBTA promotes endosomal/lysosomal escape, and thus enhances the cytotoxicity of temozolomide and improves gene silencing efficiency of siTGF- β . ALBTA significantly improves the immunosuppressive microenvironment and prolongs the survival time of glioma-bearing mice. Moreover, ALBTA can be accurately traced by MRI in brain tumors. The study indicates that this immunotherapeutic platform can serve as a flexible and powerful synergistic system for treatment with brain tumors as well as other brain diseases in central nervous system.

on surgical resection and chemotherapy. Limited by the special growth site and aggressive growth characteristics of glioblastoma, it is hard to eradicate the pathological tissue completely.^[3] Current chemotherapy mainly refers to the treatment with temozolomide (TMZ), a Food and Drugs Administration (FDA)-approved alkylating drug, to decrease the invasion of tumor cells. However, the effect of chemotherapy is severely blocked by the immunosuppressive tumor microenvironment, such as elevated levels of immune-suppressive cytokines, especially the tumor growth factor β (TGF- β).^[4]

The high level of TGF- β in tumor microenvironment inhibits T-cell and B-cell proliferation and promotes T regulatory cell proliferation.^[5] Herein, down-regulation of TGF- β has been reported as a promising approach to sensitize the TMZ-based chemotherapy via improvement of glioblastoma immune microenvironment.^[4b,6] It is well known that the specific and robust effect of RNA interference (RNAi) on gene expression renders small interfering RNA (siRNA) a valuable therapeutic agent for the down-regulation of the gene expression.^[7] Inspired by this, we propose to utilize siRNA, i.e., siRNA against tumor growth factor β (siTGF- β), to modify the immune microenvironment of glioblastoma and improve the efficacy of chemotherapy.^[8]

Glioblastoma, one of the most common primary brain tumor types of the central nervous system (CNS), is highly malignant and remains poor prognosis.^[1] The pathological hallmark of glioblastoma is the diffuse invasion of surrounding normal tissue.^[2] The traditional treatment primarily depends

Dr. C. Qiao, Dr. J. Yang, Q. Shen, R. Liu, Dr. Y. Li, Y. Shi, J. Chen, Prof. X. Zhang
State Key Laboratory of Biochemical Engineering
Institute of Process Engineering
Chinese Academy of Sciences
Beijing 100190, P. R. China
E-mail: xzhang@ipe.ac.cn

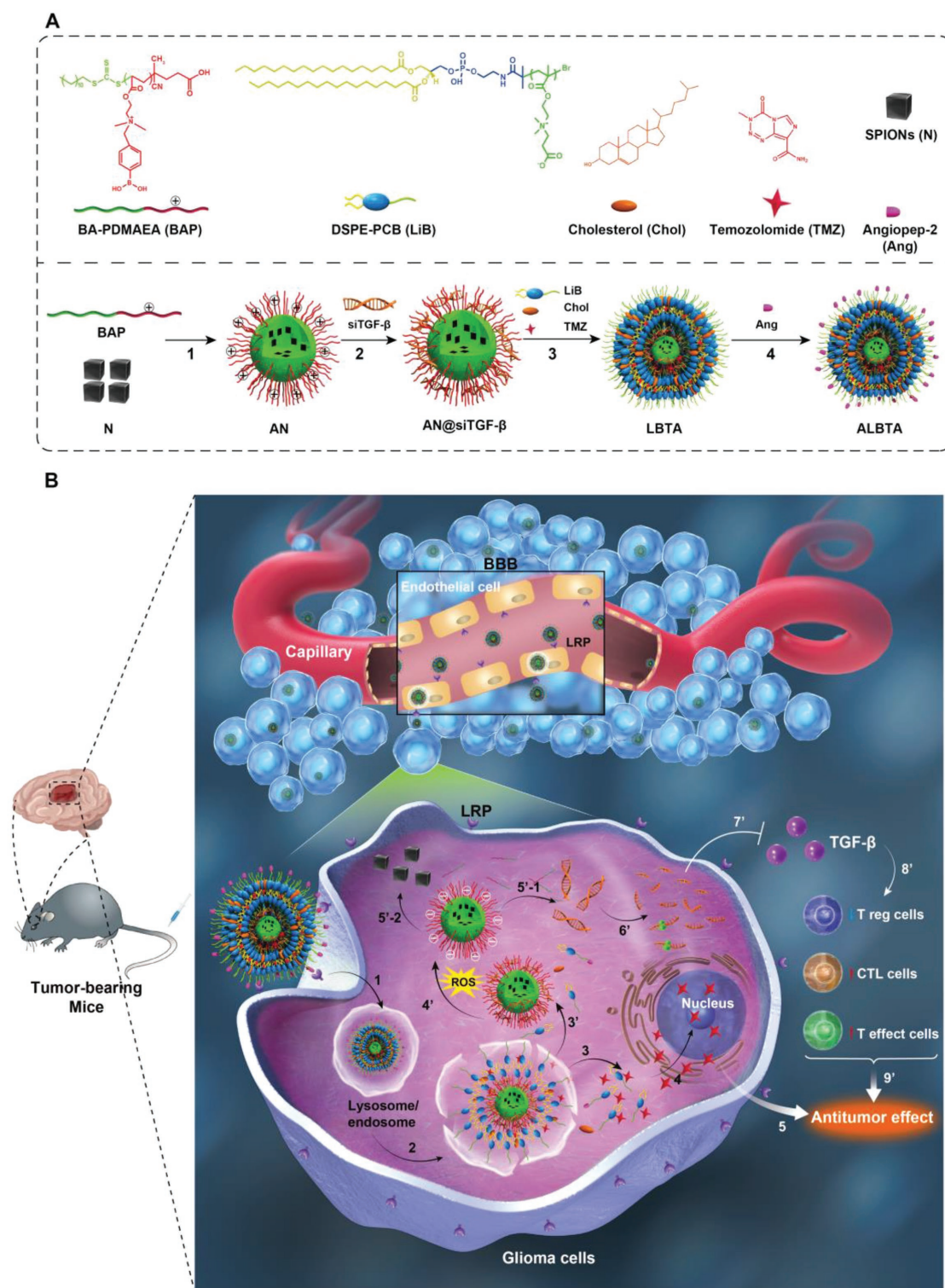
Dr. C. Qiao, Prof. J. Weng
Key Laboratory of Advanced Technologies of Materials (MOE)
School of Materials Science and Engineering
Southwest Jiaotong University
Chengdu 610031, P. R. China
E-mail: jweng@swjtu.edu.cn

Dr. C. Qiao, Prof. Y. Shen
Wuxi Medical College
Jiangnan University
Wuxi 214122, P. R. China

Prof. Z. Xiao
School of Perfume and Aroma Technology
Shanghai Institute of Technology
Shanghai 201418, P. R. China

Prof. Z. Xiao
Shanghai Research Institute of Fragrance and Flavor Industry
Shanghai 200232, P. R. China

DOI: 10.1002/adma.201705054



Scheme 1. A) Chemical structural formula of each component and preparation of the targeting nanoparticles (Ang-LiB(T+AN@siTGF- β), ALBTA). (1) BAP polymers could self-assemble into nanoparticles by encapsulating SPIONs in the hydrophobic region. (2) The positively charged AN could load siTGF- β by electrostatic attractions. (3) Then zwitterionic lipid-based envelopes were coated to the nanoparticles. (4) The targeting molecules angiopep-2 were conjugated to nanoparticles by the reaction between maleimide groups of DSPE-PCB-mal and sulfhydryl groups (-SH) of angiopep-2. B) Schematic diagram of cellular uptake and subcellular drug delivery of ALBTA. (1) The cellular uptake of targeting NPs via receptor-mediated endocytosis, (2) the acidification and perturbation with the membranes of endosomes/lysosomes, the endosomes/lysosomes escape and the release of (3) TMZ molecules and (3') nanoparticles into cytosol, (4) TMZ enter into nuclei. After being oxidized by ROS (4'), nanoparticles release (5-1') siTGF- β and (5-2') SPIONs into cytosol. SPIONs could serve as contrast agents for MRI. (6', 7') siTGF- β could down-regulate the secretion of TGF- β and (8')

However, the intrinsic deficiencies of siRNA, such as poor membrane penetrability and lack of selective targeting capability, restrict its therapeutic effects.^[9]

Given the considerations of the special location of glioblastoma, a trackable system is an ideal carrier to accurately monitor the drug trace in tumor area. Superparamagnetic iron nanocubes (SPIONs, N), which possess higher transverse relaxivity (r_2) in magnetic resonance imaging (MRI), have emerged as a new paradigm for drugs delivery applications in vivo.^[10] However, their application is severely limited by the hydrophobic character and insufficient accumulation in tumor.

To this end, we intend to establish a nanotheranostic system with RNAi-based immunotherapy for effective intracranial glioblastoma treatment. Considering the special location of the brain tumor, three challenges must be addressed: (1) the system should overcome the limitation of the blood–brain barrier (BBB) and specifically target to glioma cells; (2) the system should escape from endosomes/lysosomes effectively, avoiding degradation in late lysosomes; (3) the system should deliver TMZ and siTGF- β in a controlled manner so that they can be released into the corresponding target sites accurately.

With this concept, firstly, the dual-targeting peptide, angiopep-2, which can target the low-density lipoprotein receptor-related protein (LRP) that is overexpressed on the BBB and glioblastoma cells,^[11] is selected to guide the system for efficient targeting to intracranial glioblastoma. Secondly, the general cellular internalization pathway of nanoparticles is endocytosis, which is further trapped in lysosomes, causing efflux out of cells. Sparked by the enhanced capability of endosomal/lysosomal escape of the zwitterionic lipid distearoyl phosphoethanol-aminepolycarboxybetaine (DSPE-PCB) in our previous work,^[12] the zwitterionic-based lipid envelope (ZLE) is a preferable choice in our system. The obtained nanoparticles can improve the delivery of TMZ and siTGF- β into cytoplasm. Finally, since the intracellular signaling ROS, including H₂O₂, superoxide anions (O₂⁻), and hydroxyl radicals, is known to be elevated in cancerous cells,^[13] poly[(2-acryloyl)ethyl(p-boronic acid benzyl)diethylammonium bromide] (BA-PDEAEA, BAP), an ROS-responsive polymer, is chosen for controlled release of siTGF- β . After exposure to ROS, the reactive oxygen species can trigger the charge reversal by oxidizing benzylboronic acid/esters and elicit the release of nucleic acid molecules. Besides, considering the amphiphilic property of BAP, lipophilic SPIONs can be introduced into the hydrophobic core for MRI. Inspired by the design of nanosystem with core-shell structure, we propose the design of the following nanosystem.^[14]

As shown in **Scheme 1A**, BAP polymers could self-assemble into nanoparticles by encapsulating SPIONs in the hydrophobic region (BAP/SPIONs, AN) (1). The positively charged BAP could condense with siTGF- β to form BAP/SPIONs@siTGF- β nanoparticles (AN@siTGF- β) (2), and the zwitterionic lipid-based envelopes (ZLEs) were then coated on nanoparticles as well as TMZ to construct the nanotheranostic system (LiB(T+AN@siTGF- β), LBTA) (3). The dual-targeting peptide

angiopep-2 was conjugated with the maleimide (Mal) groups at the end of DSPE-PCB-mal to obtain the final nanosystem (Ang-LiB(T+AN@siTGF- β), ALBTA) (4).

Herein, the proposed drug-delivery route was illustrated in **Scheme 1B**, with the help of angiopep-2, the nanosystem ALBTA accumulated into the tumor region selectively after crossing BBB. After entering the glioblastoma cells via receptor-mediated endocytosis (1), the nanosystem was internalized into endosomes/lysosomes. The zwitterionic lipid DSPE-PCB gradually became positively charged as the acidic proceeding, which led to the perturbation of the membrane of endosomes/lysosomes (2), and helped TMZ (3) and AN@siTGF- β nanoparticles (3') escape into cytoplasm. The released TMZ further entered into nuclei to kill the glioblastoma cells (4) and performed antitumor effect (5). Meanwhile, the nanoparticles were triggered by the intracellular ROS (4'). Upon oxidation of the boronic acid group of BAP, the positive quaternary ammonium could change to negative carboxylic group by releasing p-quinone methide (p-hydroxylmethylenephenol) and ester bond breakage, which could facilitate the release of the bounded siTGF- β (5'-1). The down-regulation of TGF- β could modulate the glioblastoma immune microenvironment by regulating the naïve T cell (6', 7', and 8'), and eventually possessed a synergistic effect on the antitumor therapy (5 and 9'). The released SPIONs were used to trace the system through MRI (5'-2). Therefore, the nanotheranostic system (ALBTA) would be an effectively therapeutic and traceable system for intracranial glioblastoma treatment.

BAP were synthesized through reversible addition-fragmentation chain transfer (RAFT) polymerization, and conjugated with 4-(bromomethyl) phenylboronic acid to obtain the reactive oxygen species (ROS)-labile charge-reversal polymer BAP (Figure S1, Supporting Information). As a control of BAP, BB-PDMAEA (BBP) polymers without ROS responsiveness were synthesized in a similar route (Figure S2, Supporting Information). The chemical structures of the obtained polymers were confirmed by ¹H NMR (Figure S3, Supporting Information). DSPE-PCB-mal were synthesized by conjugating N-(4-Aminophenyl)maleimide (APM) with DSPE-PCB (Figure S4, Supporting Information). ¹H NMR result indicated that 10% DSPE-PCB were successfully conjugated with APM (Figure S5, Supporting Information). The oleic acid coated SPIONs were fabricated by using the thermal decomposition method with minor changes.^[10] The morphology of SPIONs was observed by transmission electron microscope (TEM) with a diameter of 23 nm (Figure S6, Supporting Information).

The BAP could be oxidized once exposed to ROS (such as H₂O₂) and then generated the negatively charged polyacrylic acid (PAA) (Figure S7, Supporting Information). The capability of ROS responsiveness of BBP and BAP was confirmed by ¹H NMR after incubating polymers with H₂O₂ solution for 0.5 h, 2 h, 8 h, and 24 h, respectively (Figure S8, Supporting Information). No peak shift was observed in BBP group, while an obvious change occurred around 6.6–7.5 ppm after 0.5 h

the down-regulation of TGF- β may further regulate the proliferation of the T cells, including T regulation cells (Treg), T effect cells (Teff) as well as cytotoxic lymphocyte (CTL). The synergistic effect could obtain by the combination of (5) the antitumor effect of TMZ and (9') the immune modulation of TGF- β . (BBB: blood–brain barrier, LPR: low-density lipoprotein receptor-related protein).

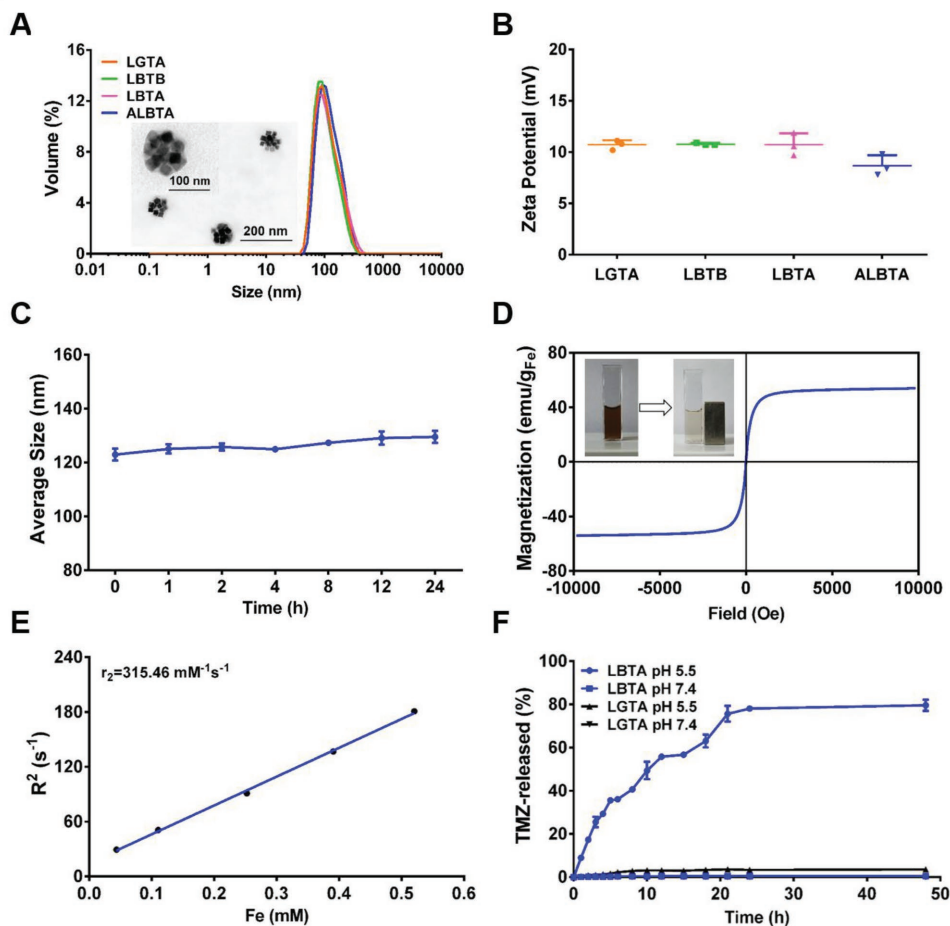


Figure 1. A) The average size of different nanoparticles at N/P ratio of 10. (The inset image is the TEM result of ALBTA, scale bar: 200 nm; ALBTA with higher magnitude is shown in the top-left corner, scale bar: 100 nm; and the polydispersity index of LGTA, LBTB, LBTA, and ALBTA were 0.143, 0.221, 0.153, and 0.229, respectively.) B) The zeta potentials of different nanoparticles dispersion in $0.01 \times 10^{-3} \text{ M}$ PBS at 25 °C. C) The serum stability of ALBTA after incubation in culture medium supplemented with 10% FBS. D) The magnetization curve of ALBTA. (The inset image showed the accumulation of ALBTA with the magnet.) E) A plot of r_2 as a function of the Fe concentration of ALBTA. The slope of Fe concentration- R_2 regression curve was r_2 relaxivity. F) The TMZ released from LGTA (black line) and LBTA (blue line) at pH of 7.4 and 5.5 at 37 °C. Data are presented as the mean \pm SD.

incubation with BAP, which verified the ROS-responsive capability of BAP.

BAP could form nanoparticles by encapsulating SPIONs through hydrophobic interaction (BAP/SPIONs, abbreviated as AN). The control nanoparticles BBP/SPIONs (BN) were prepared to investigate the effect of ROS responsiveness of BAP on the siRNA controlled release. As shown in Figure S9A in the Supporting Information, the average sizes of AN@siRNA were decreased from 135.9 to 51.3 nm as the N/P ratio increased from 0.5 to 50, which was similar to that of BN@siRNA. Meanwhile, the zeta potentials of AN@siRNA were changed from 3.18 to 51.3 mV as the N/P ratio increased (Figure S9B, Supporting Information; N: nitrogen moiety of BAP, P: phosphate groups of siRNA). This indicated that siRNA could be effectively condensed to form compact uniform nanoparticles when N/P ratio was larger than 10 (Figure S9C, Supporting Information). The r_2 values of the nanoparticles were obtained by calculating the change in the spin-spin relaxation rate (R_2) per unit iron concentration. The r_2 values of BN@siRNA and

AN@siRNA were 361.83 and 355.52 $\text{mM}^{-1} \text{ s}^{-1}$, respectively (Figure S9D, Supporting Information).

The agarose gel retardation assay was performed to evaluate the siRNA condensation capability of nanoparticles.^[15] As shown in Figure S10A in the Supporting Information, the complete retardation of siRNA was achieved at N/P ratio range from 3 to 50, suggesting that AN could load siRNA at the N/P ratio greater than 3. The siRNA condensation capability of BN was comparable to that of BN nanoparticles (Figure S10B, Supporting Information). Besides, the controlled release of siRNA from AN@siRNA was also tested by agarose gel retardation assay (Figure S10C,D, Supporting Information).^[16] The siRNA loading efficiency was evaluated by Quant-iT RiboGreen RNA Reagent and Kit (Invitrogen; Figure S11, Supporting Information). More than 95% of siRNA was complexed with nanoparticles. After incubating with H_2O_2 solution at concentration more than $0.25 \times 10^{-3} \text{ M}$ for 1 h, the siRNA could be released from AN@siRNA, while no band was observed in BN@siRNA group. Furthermore, the size variation of nanoparticles

after treatment with H_2O_2 was monitored by DLS. As per the data shown in Figure S12 in the Supporting Information, no changes happened in group of BN@siRNA whereas great increase occurred in group of AN@siRNA. The size change of AN@siRNA was due to electrostatic repulsion when oxidized by H_2O_2 . The ROS-responsive release of siRNA was further confirmed by confocal laser scan microscopy (CLSM). There was no FAM-siRNA released from the nanoparticles (red fluorescence) after inhibition of ROS with the inhibitor DPI (Figure S13A,B, Supporting Information).

To confirm the biocompatibility of the nanoparticles, the cytotoxicity at N/P ratios ranging from 0.5 to 50 was estimated by a methyl thiazolyl tetrazolium (MTT) assay. GL261 was chosen as a glioblastoma model cell. As shown in Figure S14A,B in the Supporting Information, these two nanoparticles had very low toxicity. The in vitro transfection efficiency was analyzed by flow cytometry using carboxyfluorescein (FAM)-labeled siRNA (FAM-siRNA) as a fluorescence probe in GL261 glioblastoma cells. As shown in Figure S14C in the Supporting Information, the highest transfection efficiency of

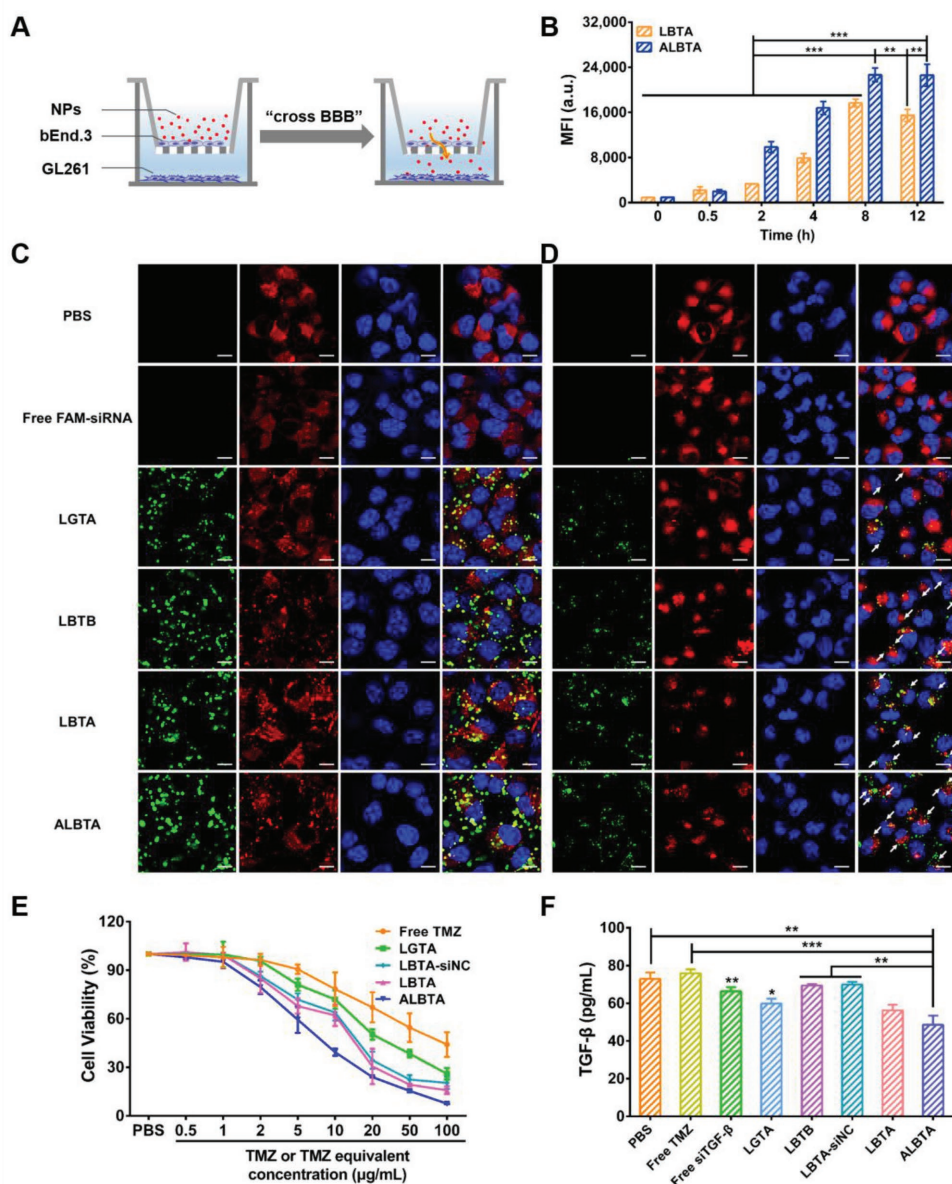


Figure 2. A) The schematic illustration of transwell model. B) The cellular uptake efficiency of LBTA and ALBTA nanoparticles after transport across the bEnd.3 monolayer. C) The cellular uptake and D) the endosomal/lysosomal escape of various formulations assayed by CLSM after incubation for 4 and 8 h, respectively. E) The cytotoxicity of GL261 cells after treatment with free TMZ, LGTA, LBTA-siNC, LBTA, and ALBTA, respectively. F) The regulation of TGF- β secretion after treatment with various formulations for 48 h in vitro. The scale bar corresponds to 20 μ m. Data are presented as the mean \pm SD. Error bars are based on triplicated experiments. *: differences between ALBTA with other groups, **: $P < 0.01$, ***: $P < 0.001$.

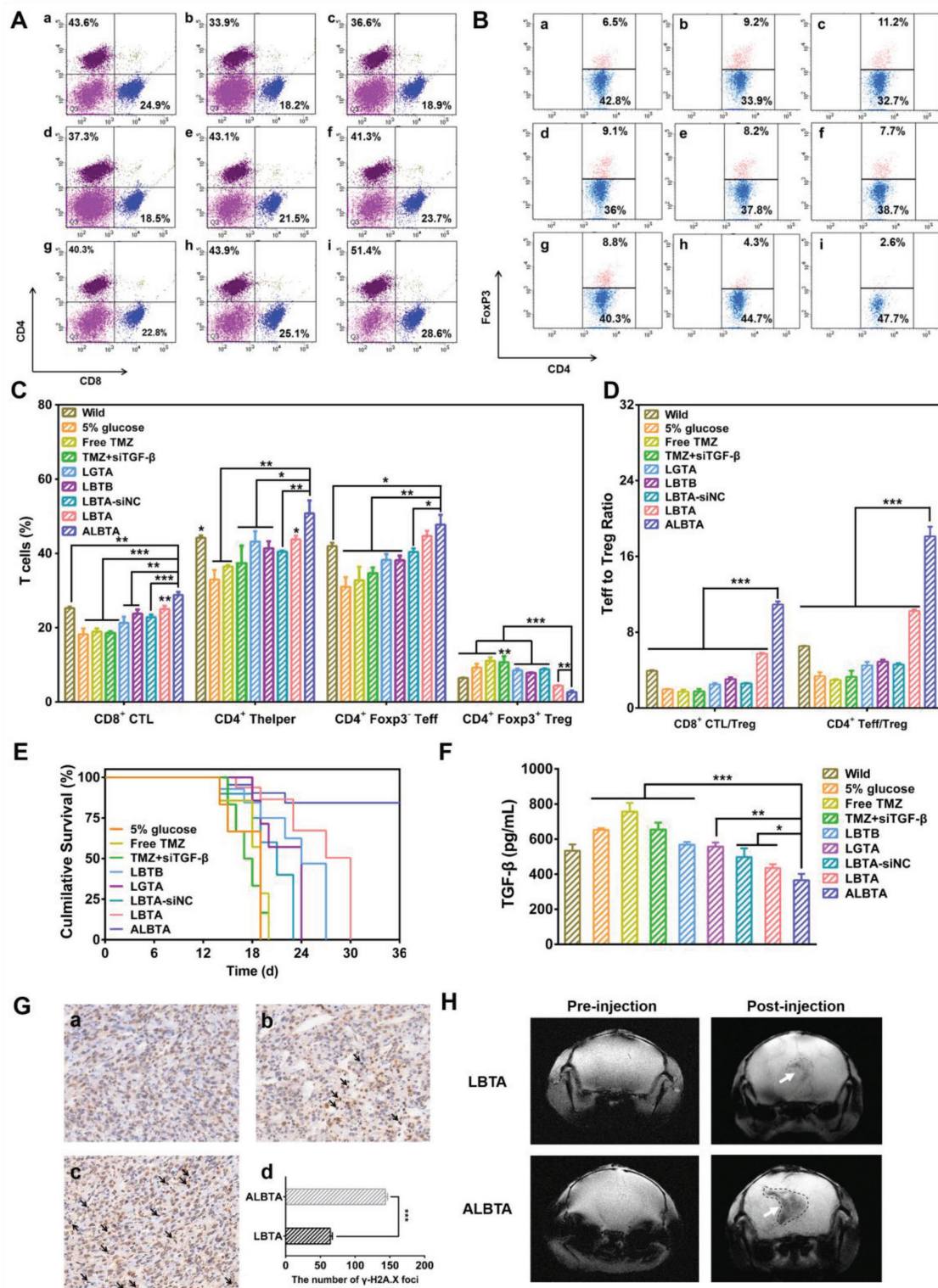


Figure 3. A) Representative flow cytometry plots showing different groups of CTL (gated on CD3⁺CD4⁻CD8⁺ cells, blue plots) and T helper cells (gated on CD3⁺CD4⁺CD8⁻ cells, wine plots) in spleen. B) Representative flow cytometry plots showing percentages of regulatory T cells (gated on CD4⁺ FoxP3⁺ cells) and effector T cells (gated on CD4⁺ FoxP3⁻ cells) in spleen after various treatments (a, wild; b, 5% glucose; c, free TMZ; d, TMZ+siTGF-β; e, LGTA; f, LBTB; g, LBTA-siNC; h, LBTA; i, ALBTA). C) Proportions of CD8⁺ CTL, CD4⁺ T helper cells, CD4⁺FoxP3⁻ effector T cells, and CD4⁺FoxP3⁺ regulatory T cells according to data in (A) and (B). D) CD8⁺ CTL: Treg ratios and CD4⁺ effector T cells: Treg ratios in spleen upon various treatments. E) The survival time of different groups of intracranial glioblastoma-bearing mice after various treatments. F) The regulation of TGF-β secretion after treatment with various formulations in vivo. G) γH2A.X staining for animals after treatment with 5% glucose, LBTA or ALBTA (a–c). 200× magnification. d) Relative

AN@FAM-siRNA was achieved at N/P ratio of 10. Taking the cytotoxicity and transfection efficiency into accounts, AN@siRNA nanoparticles with an N/P ratio of 10 were chosen in the following experiments.

The zwitterionic lipid-based envelope was introduced to encapsulate the nanoparticles and TMZ by using the thin-film method. As shown in Table S1 in the Supporting Information, LipoPCB(TMZ+BA-PDMAEA/SPIONs@siTGF- β) (LBTA) without angiopep-2 were prepared as a comparison. Non-ROS-responsiveness nanoparticles LipoPCB(TMZ+BB-PDMAEA/SPIONs@siTGF- β) (LBTB) were used to study the ROS-responsive capability. Nanoparticles with nonsense siRNA, LipoPCB(TMZ+BA-PDMAEA/SPIONs@siNegative Control) (LBTA-siNC), were used to exclude the “off-target” effect of siTGF- β . Moreover, in order to investigate the endosome/lysosome escape capability of DSPE-PCB, the neutral lipid DSPE-PEG based envelope was also prepared to form LipoPEG(TMZ+BA-PDMAEA/SPIONs@siTGF- β) nanoparticles (LGTA).

The obtained nanosystem was around 120 nm with a zeta potential of 10 mV (Figure 1A,B). The TEM image inset in Figure 1A showed that SPIONs were tended to aggregate at the center of the nanoparticles. The excellent serum stability was verified by the slight changes (\approx 10 nm increase) in average size after incubation in culture medium supplemented with 10% FBS for different time (Figure 1C). The nanosystem ALBTA exhibited good magnetic properties, with the saturation magnetization about 54 emu g⁻¹ (Figure 1D). The inset image in Figure 1D showed that ALBTA accumulated on the cup wall with a magnet, which suggested that ALBTA were magnetic field sensitive. Furthermore, ALBTA had an r_2 value of 315.46 mm⁻¹ s⁻¹, which was high enough for in vivo MRI application (Figure 1E).

The loading efficiency of TMZ was detected by using UV-vis spectroscopy with a characteristic absorption peak at 329 nm.^[17] As presented in Table S2 in the Supporting Information, the loading efficiency of TMZ was about 110.54, 95.85, 102.42, 109.34, and 106.27 μ g mg⁻¹ for LGTA, LBTB, LBTA-siNC, LBTA, and ALBTA, respectively. To investigate the release kinetics of TMZ, the NPs were incubated under different conditions for 2 d at 37 °C. The conditions of pH 7.4 and 5.5 were simulating the physiological environment and endosomes/lysosomes of tumor cells, respectively.^[18] As displayed in Figure 1F, there was only 0.52% TMZ release from LBTA at pH 7.4, indicating that the NPs were stable in culture medium, which was inconsistent with the serum stability result (Figure 1D). However, the total release of TMZ from LBTA at pH 5.5 was about 79.57% after incubation for 48 h. That indicated that the protonation of DSPE-PCB in acidic conditions disrupted the NPs and released the cargoes.^[19] The change of zeta potentials in LGTA and LBTA group at pH 7.4 and 5.5 also confirmed the capability of protonation (Figure S15A, Supporting Information), which was further confirmed by the acid-base titration experiment (Figure S15B, Supporting

Information). On the contrary, the release of TMZ from LGTA was negligible at pH 7.4. And only 3.58% of TMZ was released from those NPs after incubation even at pH 5.5 for 48 h, indicating that they displayed no responsiveness to the acid environment. Collectively, these results indicated TMZ was sustaining release in a pH-responsive manner.

Next, the in vitro BBB transport efficacy of the nanosystems was measured by using transwell filters seeded with a compact bEnd.3 monolayer to simulate the BBB (Figure 2A).^[3,20] The cellular uptake of GL261 cells was tested over a period of 12 h to indicate the transport efficiency by flow cytometry. Figure 2B revealed that ALBTA possessed the more prominent transport capability compared with LBTA. This receptor-mediated transcytosis (RMT) was further confirmed by a blocking assay.^[3] Excess free angiopep-2 was pre-incubated in the culture medium to competitively bind to LRP receptors on the in vitro BBB model, which resulted in significantly reduced transport efficiency of ALBTA to the level of LBTA (Figure S16, Supporting Information). These data strongly demonstrated the critical role of angiopep-2, which mediated transcytosis in crossing the BBB and targeting to glioma cells for ALBTA.

The cellular uptake and endosomal/lysosomal escape of different formulations were further observed by CLSM after transfection for 4 and 8 h, respectively. As shown in Figure 2C, there was a relatively high number of co-localization (yellow) for LGTA, LBTB, and LBTA, which combined the green FAM-siRNA and red endosomes/lysosomes fluorescence. Remarkably, the cellular uptake of ALBTA was 1.46 times higher than that of LBTA, which suggested that ALBTA could enhance the cellular uptake efficiently (Figure S17A, Supporting Information). This was inconsistent with the data in the in vitro BBB transport efficacy experiment (Figure 2B). After 8 h of incubation, the FAM-siRNA fluorescence was separated from the red fluorescence labeled endosomes/lysosomes in LBTB, LBTA, and ALBTA groups due to the protonation effect of DSPE-PCB in acidic environment, and the co-localization ratio was reduced by 22.1%, 21.9%, and 29.8%, respectively (Figure S17B, Supporting Information) (white arrows pointed the separated FAM-siRNA fluorescence). The much reduction of co-localization ratio in ALBTA group was related with the higher cellular endocytosis (Figure 2C). The FAM-siRNA fluorescence for LGTA was still co-localized within the endosomes/lysosomes because of the steric hindrance of DSPE-PEG, with the co-localization ratio only reduced by 6.4%. These results indicated zwitterionic NPs could facilitate enhanced endosomal/lysosomal escape. This was also in accordance with our previous research that zwitterionic liposomes could help siRNA escape from endosomes/lysosomes.^[19]

The in vitro antitumor effect of the formulations on GL261 glioblastoma cells was evaluated by MTT assay. As shown in Figure 2E, each of TMZ formulations inhibited the growth of GL261 cells. The IC₅₀ values of free TMZ, LGTA, LBTA-siNC, LBTA, and ALBTA were 80, 20, 14.62, 14, and 8 μ g mL⁻¹, respectively (Table S3, Supporting Information). The results indicated that the cytotoxicity

γ H2A.X foci number in tumor from different groups of mice based on γ H2A.X staining data shown in panel (G, a–c). H) Representative in vivo T₂*-weighted MRI images of brains in intracranial glioblastoma mice before and after injection of LBTA (upper) or ALBTA (lower). Data are presented as the mean \pm SD. Error bars are based on triplicated experiments. *: differences between ALBTA with other groups, *: P < 0.05, **: P < 0.01, ***: P < 0.001.

of TMZ was significantly increased when TMZ molecules were loaded into ALBTA nanoparticles, with 10-fold increase. The changes in the secretion of TGF- β were an important indicator of immune microenvironment, which obviously sensitized the TMZ-based chemotherapy. As shown in Figure 2F, free TMZ treatment slightly regulated the secretion of TGF- β , while the ALBTA group exhibited a significant down-regulation of TGF- β level. Reverse transcription-polymerase chain reaction (RT-PCR) was performed to validate the RNAi effect on the TGF- β expression at molecular level (Figure S18A, Supporting Information). And nonsense siRNA was also used as a control to exclude the “off-target” effect (Figure S18B, Supporting Information). To further confirm the on-target effect of RNAi on TGF- β expression, RNA rescue assay was performed after 5' rapid-amplification of cDNA ends-polymerase chain reaction (5' RACE-PCR results not shown). As shown in Figure S19 in the Supporting Information, the expression level of TGF- β in cells treated with siTGF- β could return after transfected with a siRNA-resistant TGF β cDNA (primer's information shown in Table S4 in the Supporting Information).

The T cells of immune system played a vital role for tumor therapy. For example, the cytotoxic T lymphocytes (CTL) (CD3⁺CD4⁻CD8⁺) could kill tumor cells directly; helper T cells (CD3⁺CD4⁺CD8⁻) had a great effect on the regulation of adaptive immunities.^[21] Herein, immune cells in spleen were studied on day 3 after the last injection (Figure 3A–C). The mice treated with free TMZ or TMZ+TGF- β failed to promote CD8⁺ CTL proliferation. In contrast, the percentage of CD8⁺ CTL of mice treated with ALBTA significantly increased from 18.2 to 28.6, which was higher than that treated with LGTA (21.5%), LBTB (23.7%), LBTA-siNC (22.8%), and LBTA (25.1%). Moreover, the percentage of helper T cells exhibited the same trend as CTL, with the highest promotion of 51.4% when treated with ALBTA. The effective T cells (CD3⁺CD4⁺Foxp3⁻) that were helpful to promote immune responses, and the regulatory T cells (Tregs) (CD3⁺CD4⁺Foxp3⁺) that could hamper effective antitumor immune responses were also assayed. The treatment with ALBTA could greatly reduce the percentage of Treg (\approx 2.6%, compared with \approx 9.2% in free TMZ group). Both CD8⁺ CTL/Treg ratios and CD4⁺ Teff/Treg ratios were greatly enhanced in mice after treatment with ALBTA (Figure 3D). The higher percentage of CD8⁺ CTL, CD4⁺ T helper, and T effect cells (Teff) in mice treated with LBTA than that of LBTB might be due to the ROS-responsive release of siTGF- β . The enhanced endosomal/lysosomal escape capability of LBTA resulted in much more CD8⁺ CTL, CD4⁺ T helper, and T effector cell proliferation and less Treg than that of LGTA. These indicated that the change of the immune microenvironment could facilitate the chemotherapy for glioblastoma. Similar trends were obtained from the immunofluorescence results of brain tumor section (Figure S20, Supporting Information).

The immunochemotherapeutic system had an impact on the survival time of glioma-bearing mice (Figure 3E). No significant difference was observed in the 5% glucose, free TMZ, and TMZ+siTGF- β group, while treatment with LGTA, LBTB, and LBTA prolonged the survival time of glioma-bearing mice (Figure 3E). Specifically, ALBTA-treated mice increased the medium survival time from 19 d (untreated group) to 36 d without sharp weight loss (Figure S21, Supporting Information). The level of TGF- β indicated a remarkable change for

immune microenvironment; hence, TGF- β in serum was characterized. As expected, mice treated with ALBTA shown a strong reduction in TGF- β secretion than other groups (44% reduction compared with untreated group, Figure 3F). Moreover, TMZ activity in vivo was evaluated by using immunohistochemistry (IHC). TMZ, a potent DNA damaging drug, could produce the accumulation of phosphorylated histone H2A.X (γ H2A.X), a hallmark of the DNA damage response (DDR).^[22] As shown in Figure 3G, IHC analysis of γ H2A.X verified an enhanced antitumor effect of TMZ in mice treated with ALBTA (black arrow). The results indicated that our system could efficiently modify the immunosuppress microenvironment induced by TMZ-based chemotherapy, and sensitize the antitumor effects.

The trace of the system in vivo was observed by using T_2^* -weighted MRI.^[10] Intracranial glioma-bearing mice were treated with LBTA and ALBTA via intravenous injection, respectively. The images were obtained after 12 h of injection. As shown in Figure 3H, there was an obvious contrast enhancement of MRI image in mice treated with ALBTA than that of LBTA-treated mice, indicating the efficient targeting and accurate trace of ALBTA in brain tumors. These results were further confirmed by Prussian-blue staining, indicating that SPIONs were mostly distributed in the tumor section (Figure S22, Supporting Information). ICP-MS results indicated a highly selective accumulation of ALBTA in brain tumor compared with other groups (Figure S23A,B, Supporting Information).

In summary, we have successfully established an ROS-responsive nanotheranostic platform based on RNAi-based immunomodulation. This nanosystem could (i) cross BBB via receptor-mediated transcytosis and realize active targeting, (ii) control release of drugs and contrast agents depending on the change of the local microenvironment, and (iii) trace the nanosystem for in vivo visual application. Both in vitro and in vivo results indicated that this immunochemotherapeutic system could effectively down-regulate the expression of TGF- β and dramatically enhance the efficacy of FDA-approved drug TMZ against intracranial glioblastoma. With the synergistic combination, the survival time of glioma-bearing mice was significantly prolonged. Conclusively, the proposed immunochemotherapeutic platform has great promise to serve as a flexible and powerful synergistic system for treatment with brain tumors as well as other brain diseases in CNS.

Supporting Information

Supporting Information is available from the Wiley Online Library or from the author.

Acknowledgements

C.Q. and J.Y. contributed equally to this work. This work was financially supported by the National High Technology Research and Development Program (2016YFA0200303), the National Natural Science Foundation of China (Grant Nos. 51573188, 31522023, and 51373177), the “Strategic Priority Research Program” of the Chinese Academy of Sciences (XDA09030301-3), and the Beijing Municipal Science & Technology Commission (Grant No. Z161100002616015). All procedures involving experimental animals were performed in accordance with protocols

approved by the Institutional Animals Care and Use Committee of Peking University.

Conflict of Interest

The authors declare no conflict of interest.

Keywords

immunotherapy, intracranial brain tumors, magnetic resonance imaging (MRI), temozolomide (TMZ), tumor growth factor- β (TGF- β)

Received: September 4, 2017

Revised: January 18, 2018

Published online:

- [1] a) J. T. Huse, E. C. Holland, *Nat. Rev. Cancer* **2010**, *10*, 319; b) M. Preusser, S. de Ribaupierre, A. Wohrer, S. C. Erridge, M. Hegi, M. Weller, R. Stupp, *Ann. Neurol.* **2011**, *70*, 9; c) L. Arko, I. Katsy, G. E. Park, W. P. Luan, J. K. Park, *Pharmacol. Ther.* **2010**, *128*, 1.
- [2] a) M. F. Kircher, A. de la Zerda, J. V. Jokerst, C. L. Zavaleta, P. J. Kempen, E. Mittra, K. Pitter, R. M. Huang, C. Campos, F. Habte, R. Sinclair, C. W. Brennan, I. K. Mellinshoff, E. C. Holland, S. S. Gambhir, *Nat. Med.* **2012**, *18*, 829; b) J. K. Park, T. Hodges, L. Arko, M. Shen, D. Dello Iacono, A. McNabb, N. O. Bailey, T. N. Kreisl, F. M. Iwamoto, J. Sul, S. Auh, G. E. Park, H. A. Fine, P. M. Black, *J. Clin. Oncol.* **2010**, *28*, 3838.
- [3] D. L. Ni, J. W. Zhang, W. B. Bu, H. Y. Xing, F. Han, Q. F. Xiao, Z. W. Yao, F. Chen, Q. J. He, J. N. Liu, S. J. Zhang, W. P. Fan, L. P. Zhou, W. J. Peng, J. L. Shi, *ACS Nano* **2014**, *8*, 1231.
- [4] a) A. Ksendzovskiy, D. Feinstein, R. Zengou, A. Sharp, P. Polak, T. Lichter, R. P. Glick, *J. Neuro-Oncol.* **2009**, *93*, 107; b) M. H. Barcellos-Hoff, E. W. Newcomb, D. Zagzag, A. Narayana, *Semin. Radiat. Oncol.* **2009**, *19*, 163.
- [5] a) E. Albesiano, J. E. Han, M. Lim, *Neurosurg. Clin. N. Am.* **2010**, *21*, 17; b) T. Avril, E. Vauleon, S. Tanguy-Royer, J. Mosser, V. Quillien, *Immunotherapy* **2011**, *3*, 42.
- [6] J. V. Joseph, V. Balasubramanian, A. Walenkamp, F. A. Kruyt, *Biochem. Pharmacol.* **2013**, *85*, 478.
- [7] a) C. Y. Dong, R. F. Mi, G. S. Jin, Y. Q. Zhou, J. Zhang, F. S. Liu, *Mol. Med. Rep.* **2015**, *12*, 1824; b) K. Messaoudi, A. Clavreul, F. Lagarce, *Drug Discovery Today* **2015**, *20*, 772; c) C. Sarisozen, S. Dhokai, E. G. Tsikudo, E. Luther, I. M. Rachman, V. P. Torchilin, *Eur. J. Pharm. Biopharm.* **2016**, *108*, 54.
- [8] Z. H. Xu, Y. H. Wang, L. Zhang, L. Huang, *ACS Nano* **2014**, *8*, 3636.
- [9] a) M. Van Woensel, T. Mathivet, N. Wauthoz, R. Rosiere, A. D. Garg, P. Agostinis, V. Mathieu, R. Kiss, F. Lefranc, L. Boon, J. Belmans, S. W. Van Gool, H. Gerhardt, K. Amighi, S. De Vleeschouwer, *Sci. Rep.* **2017**, *7*, 1217; b) J. Jin, K. H. Bae, H. Yang, S. J. Lee, H. Kim, Y. Kim, K. M. Joo, S. W. Seo, T. G. Park, D. H. Nam, *Bioconjugate Chem.* **2011**, *22*, 2568.
- [10] B. B. Hu, M. Zeng, J. L. Chen, Z. Z. Zhang, X. N. Zhang, Z. M. Fan, X. Zhang, *Small* **2016**, *12*, 4707.
- [11] a) H. L. Gao, S. Zhang, S. J. Cao, Z. Yang, Z. Q. Pang, X. G. Jiang, *Mol. Pharmaceutics* **2014**, *11*, 2755; b) S. B. Ruan, M. Q. Yuan, L. Zhang, G. L. Hu, J. T. Chen, X. L. Cun, Q. Y. Zhang, Y. T. Yang, Q. He, H. L. Gao, *Biomaterials* **2015**, *37*, 425.
- [12] a) Y. Li, Q. Cheng, Q. Jiang, Y. Y. Huang, H. M. Liu, Y. L. Zhao, W. P. Cao, G. H. Ma, F. Y. Dai, X. J. Liang, Z. C. Liang, X. Zhang, *J. Controlled Release* **2014**, *176*, 104; b) C. M. Qiao, J. D. Liu, J. Yang, Y. Li, J. Weng, Y. M. Shao, X. Zhang, *Biomaterials* **2016**, *85*, 1.
- [13] a) D. Trachootham, J. Alexandre, P. Huang, *Nat. Rev. Drug Discovery* **2009**, *8*, 579; b) Y. Y. Kuang, K. Baakrishnan, V. Gandhi, X. H. Peng, *J. Am. Chem. Soc.* **2011**, *133*, 19278; c) Q. Chen, C. Liang, X. Sun, J. Chen, Z. Yang, H. Zhao, L. Feng, Z. Liu, *Proc. Natl. Acad. Sci. USA* **2017**, *114*, 5343.
- [14] a) C. C. Qin, J. B. Fei, A. H. Wang, Y. Yang, J. B. Li, *Nanoscale* **2015**, *7*, 20197; b) J. X. Shao, M. J. Xuan, L. R. Dai, T. Y. Si, J. B. Li, Q. He, *Angew. Chem., Int. Ed.* **2015**, *54*, 12782; c) M. J. Xuan, J. X. Shao, L. R. Dai, Q. He, J. B. Li, *Adv. Healthcare Mater.* **2015**, *4*, 1645; d) J. Chen, J. Ding, Y. Wang, J. Cheng, S. Ji, X. Zhuang, X. Chen, *Adv. Mater.* **2017**, *29*, 1701170; e) X. Xu, P. E. Saw, W. Tao, Y. Li, X. Ji, M. Yu, M. Mahmoudi, J. Rasmussen, D. Ayyash, Y. Zhou, O. C. Farokhzad, J. Shi, *Nano Lett.* **2017**, *17*, 4427.
- [15] R. Zhang, Y. Li, B. B. Hu, Z. G. Lu, J. C. Zhang, X. Zhang, *Adv. Mater.* **2016**, *28*, 6345.
- [16] X. Liu, J. J. Xiang, D. C. Zhu, L. M. Jiang, Z. X. Zhou, J. B. Tang, X. R. Liu, Y. Z. Huang, Y. Q. Shen, *Adv. Mater.* **2016**, *28*, 1743.
- [17] a) H. Zhang, S. Gao, *Int. J. Pharm.* **2007**, *329*, 122; b) Y. Ling, K. Wei, F. Zou, S. Zhong, *Int. J. Pharm.* **2012**, *430*, 266.
- [18] a) Y. Wang, K. Zhou, G. Huang, C. Hensley, X. Huang, X. Ma, T. Zhao, B. D. Sumer, R. J. DeBerardinis, J. Gao, *Nat. Mater.* **2014**, *13*, 204; b) R. Mo, Q. Sun, J. W. Xue, N. Li, W. Y. Li, C. Zhang, Q. N. Ping, *Adv. Mater.* **2012**, *24*, 3659.
- [19] Y. Li, R. Y. Liu, Y. J. Shi, Z. Z. Zhang, X. Zhang, *Theranostics* **2015**, *5*, 583.
- [20] H. L. Xin, X. Y. Jiang, J. J. Gu, X. Y. Sha, L. C. Chen, K. Law, Y. Z. Chen, X. Wang, Y. Jiang, X. L. Fang, *Biomaterials* **2011**, *32*, 4293.
- [21] Q. Chen, L. G. Xu, C. Liang, C. Wang, R. Peng, Z. Liu, *Nat. Commun.* **2016**, *7*, 1.
- [22] E. A. Peres, A. N. Gerault, S. Valable, S. Roussel, J. Toutain, D. Divoux, J. S. Guillamo, M. Sanson, M. Bernaudin, E. Petit, *Oncotarget* **2015**, *6*, 2101.